Role of Thermally Occupied Hole States in Room-Temperature Broadband Gain in CdSe/CdS Giant-Shell Nanocrystals

Ivo Tanghe, Jordi Llusar, Juan I. Climente, Alex Barker, Giuseppe Paternò, Francesco Scotognella, Anatolii Polovitsyn, Ali Hossain Khan, Zeger Hens, Dries Van Thourhout, Pieter Geiregat, and Iwan Moreels*

Growing CdSe/CdS nanocrystals from a large CdSe core, and employing a giant CdS shell, a continuous, broadband gain spectrum, covering the spectral range between the CdSe and the CdS band edge, is induced. As revealed by $k \cdot p$ calculations, this feature is enabled by a set of closely spaced S-, P- and, for larger CdSe cores, D-state hole levels, which are thermally occupied at room temperature, combined with a sparse density of electron states. This leads to a range of bleach signals in the transient absorption spectra that persist up to a microsecond. By extending a state-filling model including relevant higher-energy states and a Fermi–Dirac distribution of holes at finite temperature, it is shown that thermal occupancy can lower the gain threshold for excited states. Inclusion of Gaussian broadening of discrete transitions also leads to a smoothening of the gain threshold spectrum. Next to a direct measurement of the gain threshold, a method is also developed to extract this from the gain lifetime, taking advantage that population inversion is limited by Auger recombination and recombination rates scale with the exciton density as $\langle N \rangle \cdot (\langle N \rangle - 1)$. The results should be readily extendable to other systems, such as perovskite or III–V colloidal nanocrystals.

1. Introduction

Two decades ago, groundbreaking work by Klimov and Bawendi demonstrated that colloidal CdSe nanocrystals display optical gain and stimulated emission at densities of about 2 excitons per quantum dot,[1] despite efficient Auger recombination.[2] This finding sparked a vivid search for new solution-processed gain materials based on colloidal quantum dots, where subsequent progress produced CdSe/CdS nanocrystals with suppressed Auger recombination,[3] microsecond pulsed[4] to continuous-wave lasing,[5] and most recently gain and lasing at sub-single-exciton densities using photo- or electrochemically charged nanocrystals.[6,7] Having reached these milestones, an outstanding challenge is to achieve such features over a wider gain bandwidth, in order to further broaden the opportunities that solution-processed gain materials

I. Tanghe, A. Polovitsyn, A. H. Khan,[+] Z. Hens, P. Geiregat, I. Moreels
Department of Chemistry
Ghent University
Gent 9000, Belgium
E-mail: iwan.moreels@ugent.be
I. Tanghe, D. Van Thourhout
Photonics Research Group
Ghent University
Gent 9000, Belgium

The ORCID identification number(s) for the author(s) of this article can be found under https://doi.org/10.1002/adom.202201378.

[+]Present address: Institute of Nano Science and Technology, Knowledge City, Sector 81, Mohali 140306, India

I. Tanghe, Z. Hens, D. Van Thourhout, P. Geiregat
Center for Nano and Biophotonics
Ghent University
Gent 9000, Belgium
J. Llusar, J. I. Climente
Departament de Química Física i Analítica
Universitat Jaume I
Castelló de la Plana 12080, Spain
A. Barker, G. Paternò
Center for Nano Science and Technology
Istituto Italiano di Tecnologia
Milano 20133, Italy
G. Paternò, F. Scotognella
Physics Department
Politecnico di Milano
Milano 20133, Italy
A. Polovitsyn, A. H. Khan, I. Moreels
Chemistry Department
Istituto Italiano di Tecnologia
Genova 16163, Italy

**ADVANCED
SCIENCE NEWS**

www.advancedsciencenews.com

**ADVANCED
OPTICAL
MATERIALS**

www.advopticalmat.de

provide for the fabrication of coherent light sources across the visible and near-infrared spectrum, as well as to enable new directions of applications, for instance in optical metrology where frequency combs based on broadband lasers are a key enabling technology.

Different groups have already reported on the observation of spontaneous multiexciton emission, as well as stimulated emission from higher-energy excited states, in particular using CdSe/CdS nanocrystals with a so-called giant shell (shell thickness ≥ 4–5 nm).[8–11] Recent work by the Bawendi group added more depth to these results,[12] by showing that spontaneous emission from P-states is strongly outcompeted by S-state emission for triexcitons in CdSe/CdS nanocrystals due to a reduced electron–hole overlap. Still, the broadened spontaneous and stimulated emission spectra observed earlier clearly imply that it is possible to open up the gain bandwidth. At the same time, the photophysics underlying the required massive population inversion has remained elusive. For instance, the influence of the thick CdS shell, resulting in strong electron delocalization and reduction of quantum confinement on the electron states, on the energetic position of excited electron and hole levels, as well as the associated optical transitions and state degeneracies remains unresolved. This for instance raises the question of how excited-state lifetimes evolve under intense excitation fluencies, where Auger recombination dominates the carrier dynamics.

In this manuscript, we present an investigation of the photophysics that underlies the population inversion and excited-state stimulated emission, recently observed in giant-shell nanocrystals with a pure-phase wurtzite crystal structure.[8] Using transient absorption spectroscopy with a time range from femto- to microseconds, we demonstrate that all transitions that are observed between the CdSe and the CdS band edge are long-lived, with a lifetime up to 1 µs, in contrast with earlier results on CdSe nanocrystals, where hot carriers rapidly relax to the CdSe band edge.[13] We demonstrate that the long lifetime finds its origin in closely spaced, thermally accessible hole states near the top of the valence band. Next, at high pump fluency, a first blue shifted gain peak is formed around 625–650 nm depending on the core diameter, with gain lifetimes extending beyond 500 ps. At increased fluencies, we were able to obtain broadband gain that includes higher states down to the CdS adsorption edge at 500 nm. For these states, the exciton density at the gain threshold fluency scales as expected for state-filling of the higher excited electron states only, resulting in a threshold that is markedly lower than what is anticipated from the high degeneracy of hole states. The gain lifetime across the spectrum evolves with the exciton-dependent Auger recombination as $\langle N \rangle \cdot (\langle N \rangle - 1)$,[14] yielding a final 7–13 ps lifetime for the highest observable state at 525–540 nm. Simulations of the gain threshold using the CdSe/CdS band structure obtained from $k \cdot p$ calculations in combination with an extended state-filling model highlight the importance of thermal occupation of excited hole states for lowering the gain threshold for specific states across the spectrum. Experimental and theoretical data reveal that broadband gain is enabled by the growth of a thick CdS shell, promoting electron delocalization, as well as employing a relatively large CdSe core, beneficial for increasing the hole density of states, yielding a

band of thermally accessible hole states in combination with a sparse density of electron states.

2. Results and Discussion

2.1. Low-Fluency Transient Absorption Spectroscopy

For this study, we have investigated two samples of CdSe/CdS pure-phase wurtzite nanocrystals with a thick CdS shell. The first has a 4.1 nm CdSe core and an overall diameter of 15.0 nm (15 monolayer, ML, CdS shell, sample A), the second has a 7.5 nm core and an overall diameter of 13.5 nm (8.6 ML CdS shell, sample B). Associated transmission electron microscope images, absorbance and PL spectra were reported previously.[8] The samples have a band gap at 636 and 646 nm, respectively (**Figure 1**). Using second-derivative analysis of the absorption spectrum,[15] we can discern up to three (sample A) and four (sample B) transitions. These transitions yield, as discussed by Di Stasio et al.,[8] amplified spontaneous emission (ASE) resulting in an ASE spectrum that extends from the CdSe core to the CdS shell band edge (**Table 1**).

In order to understand the photophysics behind the ASE spectra, we first performed transient absorption (TA) spectroscopy, in a time domain extending from femto- up to microseconds. Samples were excited with a 400 nm femtosecond pulse and the TA was collected up to 3 ns, and with a 355 nm nanosecond pulse for which the TA was collected up to 10 µs. In **Figure 2**, for sample A, both maps were normalized at 1 ns in order to reconstruct the entire decay. The excitation fluency was kept at 65 µJ cm^{-2}, for which we excite on average $\langle N \rangle \approx 1.6$ excitons per nanocrystal. We observed a broad bleach band consisting of several transitions, which all have TA bleach dynamics that extends into the microsecond time domain (Figure 2b). Independent of the wavelength interval that we probed, all transitions have a similar long-lived decay constant (Figure 2c), which also matches well with the photoluminescence decay. Note that an initial fast relaxation (2 ps time range) is observed for the 470–500 nm interval, with a similar rise time for the remaining spectral range below the CdS band edge. It
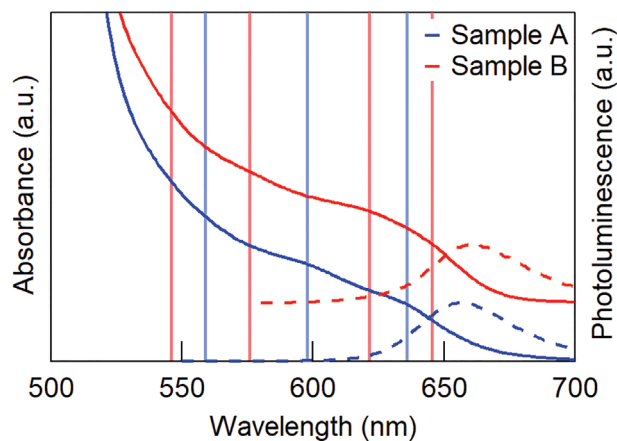

Figure 1. Absorbance spectra of the two samples, with vertical lines indicating the different transitions as obtained from second-derivative analysis. PL spectra show a maximum at 657 and 661 nm, respectively.

Table 1. Spectral position of the transitions in the absorbance and (reported[8]) ASE spectra. All ASE peaks are blue-shifted compared with the corresponding absorbance peaks.

	Sample A		Sample B	
	Absorbance [nm]	ASE [nm]	Absorbance [nm]	ASE [nm]
First peak	636	623	646	648
Second peak	598	568	622	612
Third peak	559	523	576	566
Fourth peak	–	–	546	538

reflects hot carrier relaxation to the CdS band edge.[16] A similar long lifetime is observed for all states that are probed in sample B (Figure 2d,e).

As a Stark shift, due for example to trapped charges, is expected to induce an asymmetric bleach signal with strong photoinduced absorption,[17] which we do not observe, we can rule it out as the origin of these long-lived features. Hence, they can be ascribed to state filling of different excited electron and hole levels.

2.2. Energy Level Calculations

To gain further insight into this optical behavior, we performed $k \cdot p$ band structure calculations, for a series of nanocrystals with fixed CdSe/CdS diameter of 15 nm, and for two additional CdSe/CdS that match the geometry of our experimental samples A and B. We calculated the electron and hole states within a wurtzite description. Electron states were described with a single-band effective mass Hamiltonian, for the hole states we used Chuang's six-band Hamiltonian.[18,19] Coupling between heavy hole, light hole and split-off subbands was hence taken

into account, along with a finite band offset between core and shell. As compared to cubic and quasi-cubic Hamiltonians, the wurtzite model provides a more accurate description of the density of hole states, which are significantly influenced by band coupling (see Supporting Information for a comparison). Strain and piezoelectricity[20] were not considered here (see Supporting Information for further motivation), and parameters used for the wurtzite description are given in Tables S1 and S2 (Supporting Information).

We first considered nanocrystals with fixed overall (i.e., core plus shell) diameter D_{cs} = 15 nm (similar to the experimental samples) and variable core diameter D_c (**Figure 3**a). Calculations show that electron $1S_e$ and $1P_e$ energy levels are considerably split, by 80 meV or more across the entire range (Figure 3b). Remarkably, despite the large CdS shell yielding a 15 nm overall diameter, the $1P_e$, $2S_e$ and $1D_e$ levels are also clearly split, even though they lie above the conduction band offset and are delocalized over the entire core/shell nanocrystal (Figure S2, Supporting Information) for most core diameters. The hole energy levels on the other hand are much more closely spaced (Figure 3c). A first band of states is formed by the $1S_{3/2}$ and $1P_{3/2}$ states. Due to the crystal field of the wurtzite lattice, the four-fold degenerate $1S_{3/2}$ hole state (F = 3/2, F_z = ±3/2, ±1/2) splits into a ground state doublet with F_z = ±3/2 and an excited state with F_z = ±1/2. The former (latter) has predominant heavy hole (light hole) character. Interestingly, for the experimental nanocrystals used (Figure 3d,e), these states lie within 42 and 23 meV for samples A and B, respectively, implying that these are thermally occupied at room temperature. For sample B, a second band of thermally accessible hole energy levels formed by $1P_{5/2}$ and $2S_{3/2}$ states can be identified, lying around 29–38 meV below the ground state.

The spectral position of optically allowed transitions between these states and the respective $1S_e$ and $1P_e$ electron states was
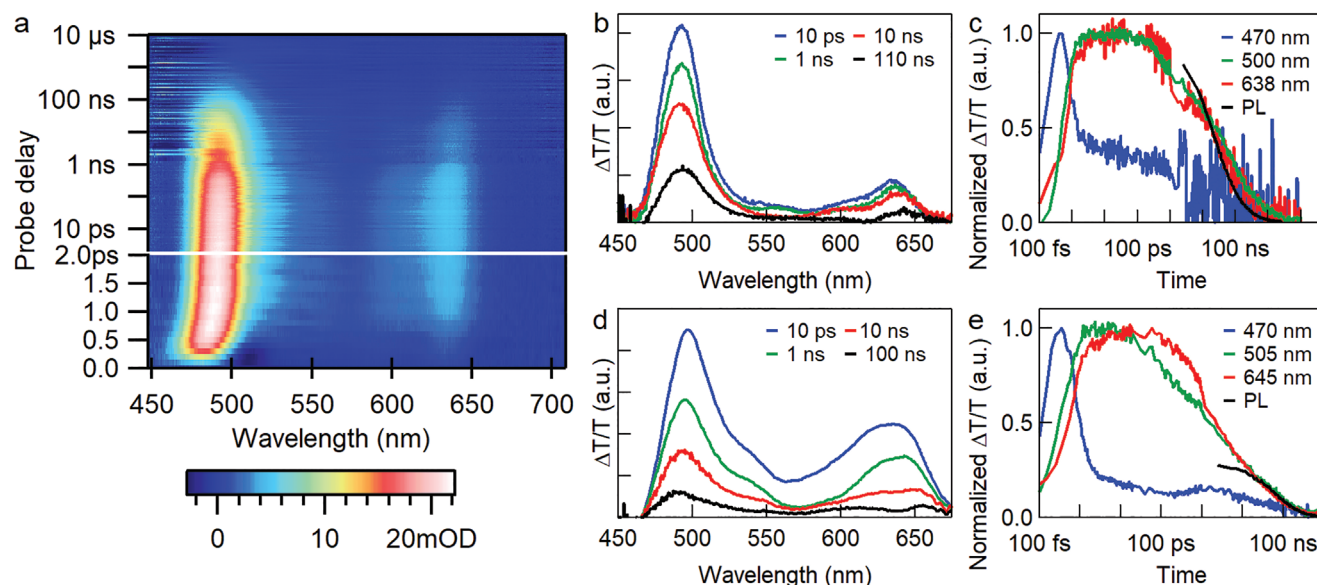

Figure 2. a) TA map for sample A, using a pump fluency of 65 μJ cm^{-2}, constructed from fs and ns excited TA spectra. b) Differential transmission $\Delta T/T$ spectra at different time intervals for sample A, demonstrating broadband, long-lived TA relaxation. c) Sample A decay traces for the TA bleach features are similar across the spectrum, and agree with the PL decay (black line). d,e) $\Delta T/T$ spectra at different delay times and decay traces for sample B, showing similar behavior.
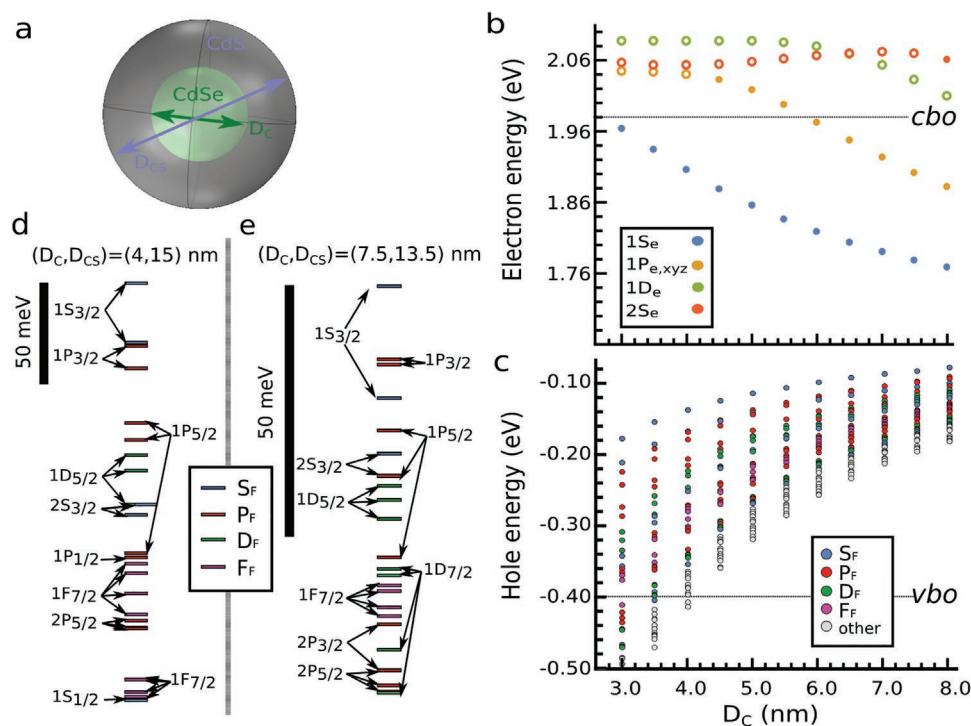
Figure 3. Calculated energy levels of wurtzite CdSe/CdS nanocrystals as a function of core diameter. a) Sketch of the heterostructure under study. b) Electron states, for which solid dots (empty circles) denote electron states with most of its charge density in the core (shell). c) Hole states. d,e) Zoom of hole states for sample A and B, respectively. In (b) and (c), energies are referred to the top of the CdSe valence band (in bulk), the dot color indicates the lowest envelope angular momentum, and the dashed line represents the bulk conduction (*cbo*) and valence (*vbo*) band offset.

subsequently calculated. We have to remark that these do not exactly match experimental values, as we did not include electron–hole Coulomb interactions in the band structure calculations. Rather than evaluating the exact Coulomb energy for the whole band of excited states, which would require massive configuration interaction calculations, we added a fixed shift to the calculated transitions, of 177 and 20.5 meV for samples A and B, respectively, to match the experimental $1S_e$-$1S_{3/2}$ transition. Resulting transition wavelengths and associated thermal occupancy of the respective hole levels are compared to the TA spectrum collected at 1 ns in **Figure 4**, with all calculated transitions reported in Tables S4 and S5 (Supporting Information). The results demonstrate that indeed, a broad range of transitions, spanning the region between the CdSe and CdS band edge, are governed by thermally occupied S- and P-hole states. In line with earlier TA experiments of the Houtepen group,[21] in high-quality CdSe/CdS nanocrystals also holes contribute to the TA bleach spectrum, hence the thermal occupation of excited hole states between the CdSe and CdS band gap is expected to yield long-lived bleach features, in agreement with experimental data. With a valence band offset between CdSe and CdS of about 440 meV, the close spacing of hole states is dictated predominantly by the large diameter of the CdSe core, showing the importance of increasing the latter to obtain the unique features described above. For sample A, we also observe a bleach feature around 600 nm that cannot be explained by the hole occupancy, however, this wavelength range corresponds to transitions involving the $1S_e$ electron state (Figure 4a, grey bars, with arbitrary height). Similar transitions appear for sample B around 635 nm.

2.3. Optical Gain Measurements

With this detailed understanding of the CdSe/CdS giant-shell band structure and TA lifetimes in the CdSe–CdS band-edges spectral range, we progressed to higher pump fluency, focusing now on femto- to nanosecond TA to investigate the gain dynamics. We measured the differential absorption ΔA at varying fluency, from which we calculated the gain G as $-(\Delta A + A_0)$, with A_0 the linear absorbance. The region of positive gain is then plotted in a gain map. **Figure 5**a shows a typical example, for sample A, measured at a pump fluency of 1.7 mJ cm^{-2}, corresponding to an exciton density of $\langle N \rangle = 18$. The maps are then time-integrated over the full time domain (up to 3 ns) to construct the gain spectrum. Figure 5b,c shows the gain spectra for sample B, and Figure 5d,e for sample A. Notice that a gain band up to 200 nm wide can be obtained, spanning essentially the entire spectral region between the CdSe and CdS band gap. While the gain spectrum is blue-shifted from the fundamental absorption gap, the wide spectral range obtained can be attributed to the ability of our CdSe/CdS to display gain even at exciton densities approaching $\langle N \rangle = 200$ for the highest pump fluency, suggesting that the large-core, giant-shell CdSe/CdS heterostructure can accommodate a high carrier density. At the same time, due to the giant-shell motif, the gain coefficient in the CdSe spectral region remains modest compared to literature values obtained on CdSe/CdS.[22] Depending on the excitation conditions the band edge gain coefficient at 3 ps is about 400–465 and 465–580 cm^{-1} for samples A and B, respectively (Figure S10, Supporting Information), while CdSe/CdS with a
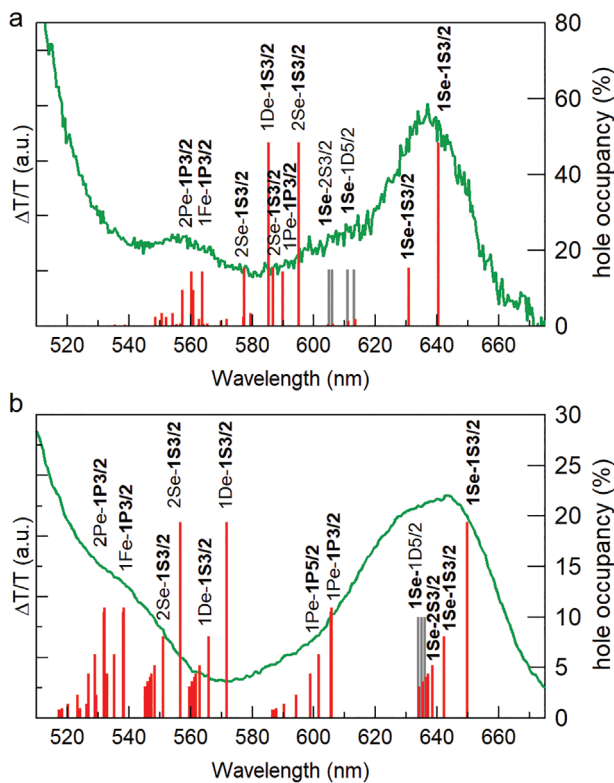
Figure 4. Calculated transitions and fractional hole occupancy (red bars) for a) sample A and b) B, compared to the experimental TA spectrum collected at 1 ns (green). Hole states that are thermally occupied (occupancy of at least 20% compared to the lowest $1S_{3/2}$ state) are marked in bold. Additional calculated transitions associated with the $1S_e$ electron state are marked with grey bars (arbitrary height).

thin shell showed values up to 2800 cm^{-1}. For higher-energy states, the gain coefficient does increase further, reaching 690 and 1090 cm^{-1} at 530 nm for samples A and B, respectively.

Next, the experimental gain spectra are compared to the spectral positions of the ASE peaks (Table 1, Figure 5, black vertical lines). Clearly, the spectral features observed in the gain spectra agree well with the spectral position of the ASE peaks. In addition, we can now also assign the states that pertain to these features. For this, we calculated the expected transition wavelength of the different states using the $k \cdot p$ band structure (Figure 5, grey vertical lines, and Tables S4 and S5, Supporting Information) for all transitions and wavelengths. Again, we applied a fixed red shift, of 137 and 26.4 meV for samples A and B, respectively, to match calculated transitions with the experimental band-edge gain peaks. Focusing first on the large-core sample B (Figure 5b,c), comparison of computational and experimental data shows that a continuous gain spectrum can indeed be obtained due to the high number of electron/hole states with transitions between the CdSe and CdS band gap. A more careful inspection shows that states which line up with the ASE/gain peaks correspond to transitions involving the $1S_e$, $1P_e$, $1D_e$, and $1F_e$ electron states, respectively. More specifically, they are due to the transitions $1S_e$-$1S_{3/2}$, the $1P_e$-$1P_{3/2}$ – $1P_e$-$1P_{5/2}$ manifold, $1D_e$-$1S_{3/2}$ – $1D_e$-$1S_{5/2}$ manifold, and $1F_e$-$1P_{3/2}$, with possible contribution from the $2P_e$-$1P_{3/2}$ – $1P_e$-$1P_{5/2}$ manifold

for the latter, as these are closely spaced with the former. For sample A, a similar picture arises, yet assignment of the final ASE transition around 520 nm (Figure 5d) remains more ambiguous, possibly due to the fact that we do not take the additional blue shift due to multiexciton repulsions into account in our $k \cdot p$ calculations. Indeed, this results in an experimental ASE transition that is not superposed on the corresponding $1F_e$-$1P_{3/2}$ transition as in the case of sample B, as this is calculated to lie around 550 nm. Note also that the gain spectra show additional features not perceived in the ASE spectra,[8] for instance around 590 and 540–550 nm. However, the absence of ASE for sample A at these wavelengths might simply be due to mode competition between the different ASE modes.

Regarding the gain threshold, for sample B, when using 530 nm excitation (Figure 5b) to avoid nonradiative carrier losses due to surface trapping, the band-edge gain develops with an onset of about $\langle N \rangle = 1$–2 excitons per nanocrystal, in line with earlier results on CdSe/CdS nanocrystals with a thinner CdS shell.[22] The excited-state gain bands develop around $\langle N \rangle = 3$ excitons for the second band, and at $\langle N \rangle = 7$–13 for the third gain band. Sample A shows a similar behavior (Figure 5d). These values are small considering the high degeneracy of hole states, and suggest that exceeding population inversion of the corresponding electron levels is sufficient to obtain gain. When extending the pump wavelength from 530 to 400 nm and thus exciting primarily the CdS shell, for sample B (Figure 5c) the exciton density for a similar gain threshold is about twice the number required when pumping the CdSe core with 530 nm excitation. In addition, the fourth gain peak appears when the exciton density exceeds $\langle N \rangle = 24$. In the small-core sample A, the core-to-total nanocrystal volume ratio is significantly smaller (1:49, compared to 1:6 for sample B), and as a result, while the same features can be observed, the exciton densities required to achieve gain using a 400 nm pump wavelength are significantly higher (Figure 5d), likely due to increased carrier trapping and nonradiative losses at the CdS surface.[23]

To understand this threshold behavior, we first measured the gain threshold by independent means. Starting with sample B, in **Figure 6**a we plot contours of the gain threshold for varying pump fluency in a time-wavelength map, using a 530 nm pump wavelength. This representation reveals that, once the maximal gain is reached, the gain lifetime τ_G, i.e., the time delay at a given wavelength for which net stimulated emission turns into net absorption, is largely independent of the pump fluency. Maximum values lie around $\tau_{G,XX} = 650$ ps for the band-edge gain. This gain lifetime is more than an order of magnitude shorter than the biexciton lifetime of $\tau_{XX} = 33$ ns estimated from the fluorescence decay time via $\tau_{XX} = \tau_X/4$,[24] allowing us to conclude that the gain lifetime is limited by nonradiative Auger recombination and not by its intrinsic radiative rate.

While ample literature is available that discusses the influence of the nanocrystal volume and the CdSe/CdS interface on the Auger rate k_{AR},[3,24–26] less is known about the scaling of k_{AR} with electron and hole density. Recently however, Philbin and Rabani[27,28] showed that electron–hole correlations should not be neglected when calculating k_{AR} in weakly to moderately confined systems including CdSe/CdS nanocrystals, leading to an Auger rate that scales not with $\langle N \rangle^2 \cdot (\langle N \rangle - 1)$, but as $k_{AR} \sim \langle N \rangle \cdot (\langle N \rangle - 1)$. Since we can assume that τ_G is inversely

ADVANCED
SCIENCE NEWS
www.advancedsciencenews.com

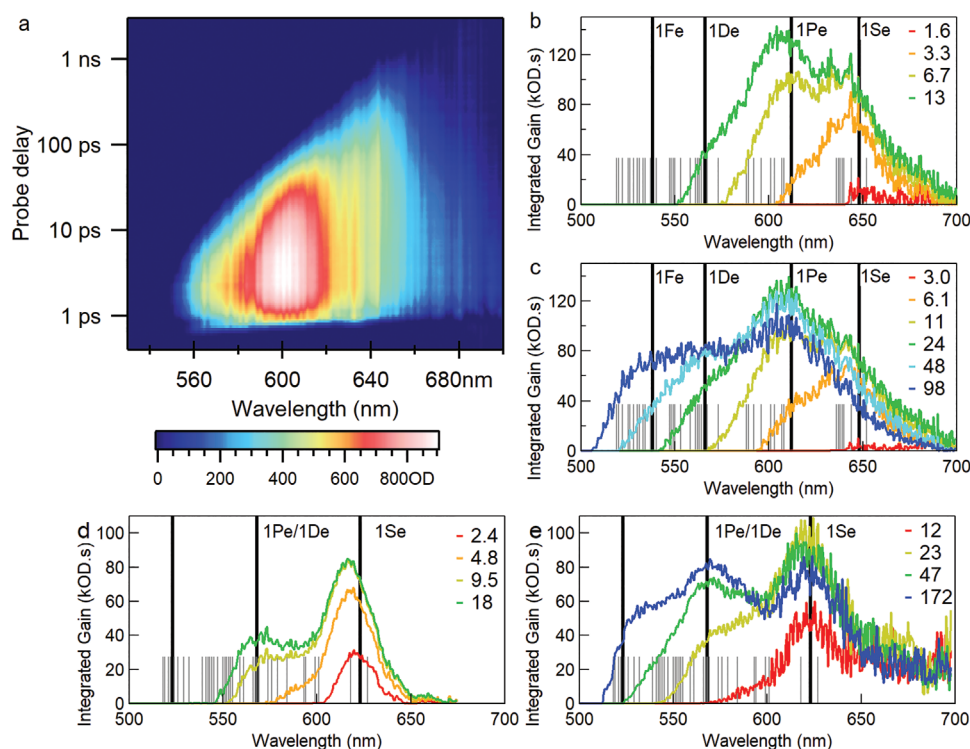ADVANCED
OPTICAL
MATERIALS
www.advopticalmat.de

Figure 5. a) TA gain map for sample A, obtained with a pump fluency of 1.7 mJ cm^{-2}. b) Time-integrated gain spectra (the spectral region that does not show gain is set to zero), exciting sample B at 530 nm. The pump fluency has been converted to a number of excitons per nanocrystal, via the linear absorption cross section. Vertical black lines correspond to the ASE peak wavelengths, see Table 1. Vertical grey lines correspond to the calculated transitions. c) When exciting sample B at 400 nm, a similar result is obtained, yet at higher exciton density. Due to the higher excitation photon energy, a fourth gain peak appears at the highest fluencies. d,e) Similar results are obtained for sample A.

proportional to k_{AR} as discussed above, the lifetime spectrum can be converted to a gain threshold spectrum using this relation, since

$$\tau_G^{-1} \sim \langle N \rangle \times (\langle N \rangle - 1) \tag{1}$$

Knowing this, when we fix the biexciton gain threshold $\langle N_{XX} \rangle$ to 1.6 as given by the direct gain threshold measurement, and the associated biexciton gain lifetime $\tau_{G,XX}$ to 650 ps as given by the gain lifetime measurement, Equation (1) gives us the threshold for any given wavelength $\langle N(\lambda) \rangle$ from the gain lifetime $\tau_G(\lambda)$ as a solution of:

$$\frac{N(\lambda) \cdot (N(\lambda) - 1)}{N_{XX} \cdot (N_{XX} - 1)} = \frac{\tau_{G,XX}}{\tau_G(\lambda)} \tag{2}$$

In Figure 6b, we compare the direct measurement of $\langle N \rangle$, extracted from an interpolation of the fluency-dependent measurements of Figure 5b (red markers), and $\langle N \rangle$ obtained from the gain lifetime using the trace collected at highest fluency in Figure 6a and Equation (2) (blue markers). A remarkable agreement is observed, highlighting both that the gain is Auger-limited, and, more importantly, that a measurement of the gain lifetime provides a powerful method to understand the exciton density at which gain develops for different wavelengths and associated electronic states. Sample A, which has a

maximal gain lifetime $\tau_{G,XX} = 495$ ps with a corresponding gain threshold $\langle N_{XX} \rangle = 1.6$, shows a similar result (Figure 6c,d).

2.4. Optical Gain Modeling

Finally, to consolidate the experimental results, the $k \cdot p$ energy level structure of the two samples was used in a state-filling scheme, to model the gain threshold for the different calculated electronic states. First, we expanded on recent state-filling models for the biexciton gain in CdSe/CdS nanocrystals,[22] here including all states calculated for our nanocrystals and their energetic position (see Tables S4 and S5 in Supporting Information). As we know from the low-fluency TA spectroscopy, lowest-lying hole states are thermally occupied at room temperature, so we added temperature as a parameter. Based on the number of carriers in the system and the temperature, the occupancy of the energy levels was calculated for both electrons and holes by applying the appropriate Poisson and Fermi–Dirac statistics (see Supporting Information Section 3 on gain modeling). Using these occupancies, we calculated the gain threshold for every transition, and together with the associated wavelength, reconstructed a discrete threshold spectrum. The latter is shown in Figure 6b,d, for samples B and A, respectively. Focusing on sample B, initially, at 0 K we obtained the case of pure sequential state filling, with a band-edge gain threshold starting at 1.15 excitons, in line with earlier
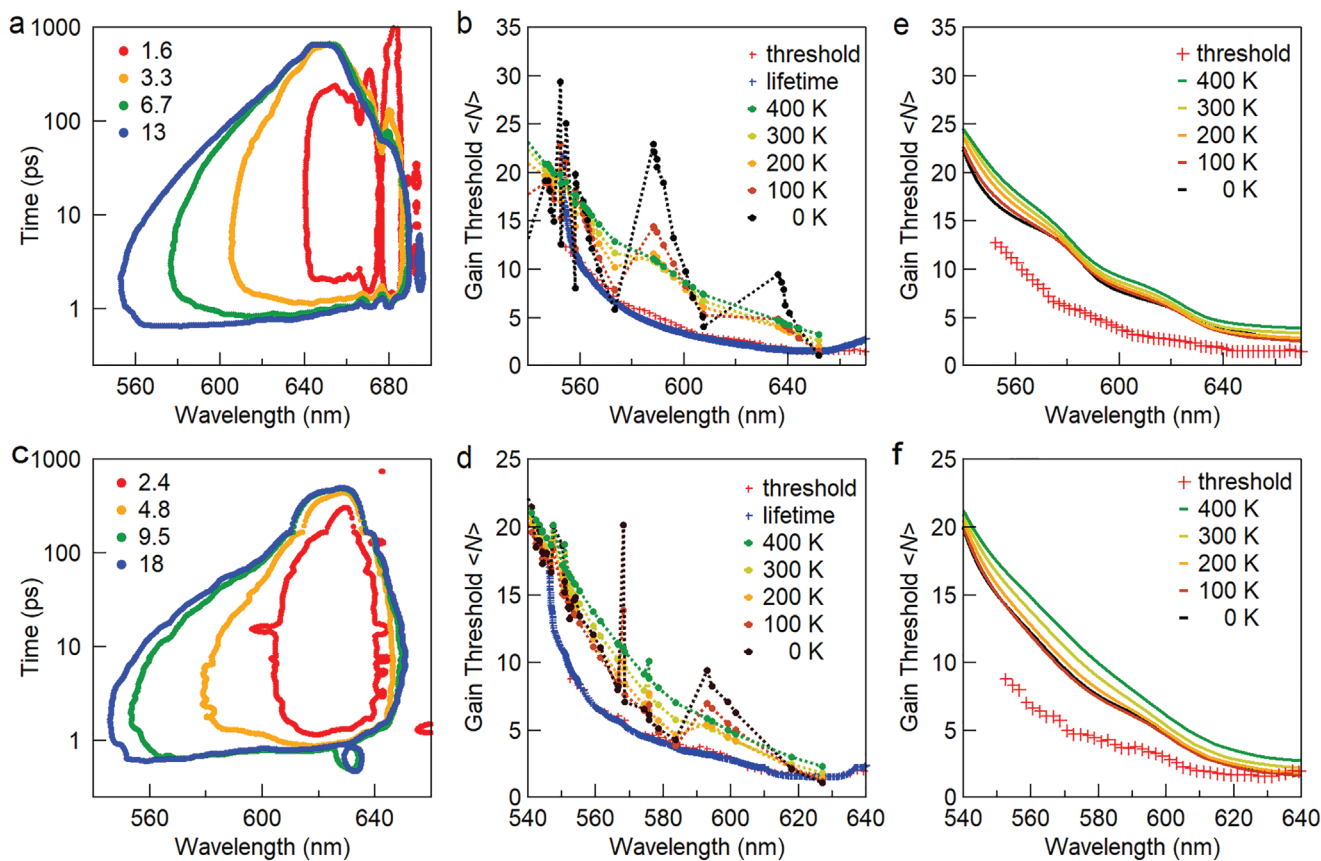
Figure 6. a) Gain lifetime spectra for sample B, plotted as contours of the gain threshold in a time-wavelength map, using an excitation wavelength of 530 nm. The legend indicates the corresponding average number of excitons per nanocrystal. b) Gain threshold spectrum obtained from direct measurement of the threshold using varying fluency (red markers), and as calculated from the gain lifetime at highest fluency (blue markers). Black, brown, orange, yellow and green traces show the gain threshold calculated from the $k \cdot p$ energy levels, at various temperatures. Due to thermal occupation of excited hole states at elevated temperature, a smoothened curve is obtained. c,d) Same data for sample A. e) Gain threshold spectra at varying temperature of sample B, calculated assuming a 75 meV line broadening for each transition. Data are compared to the experimental gain threshold (red markers). f) Same data for sample A.

results.[22] At shorter wavelengths, the gain threshold rapidly increases due to the presence of higher excited hole states, after which another low-lying threshold is observed around 610 nm, here associated with the $1P_e$-$1P_{3/2}$ transition. The pattern of increasing and decreasing threshold then repeats again. At higher temperatures however, here simulated between 100 and 400 K, we observe fewer variations in the calculated curves, due to thermal occupancy of holes in excited states. In particular, transitions associated with the lowest $1S_{3/2}$ hole state, for sample B around 650 nm, see an increase of the threshold due to a relative depletion of the hole state induced by thermal redistribution of holes over different states, while the states at slightly shorter wavelength see a strong decrease of the threshold by thermal filling of the associated hole states, leading to a more efficient population inversion for these transitions than expected from pure sequential state filling. While we acknowledge that absolute values of the calculated threshold still remain about a factor of two higher than experimental data, the gradual increase of the gain threshold toward shorter wavelength is in line with the experimental observations. Hence, at a small cost of increasing the gain threshold at the band edge, where hole states are depleted by thermal excitation, we can

strongly reduce the gain threshold at higher energies by taking advantage of the same thermal excitation of holes into higher-excited states. Sample A shows similar behavior.

Second, as we also know that the nanocrystal ensemble exhibits absorption features that are broadened at room temperature, also the influence of line broadening was assessed. To do so, a line width of 75 meV was assigned to each transition, in accordance with the line width of the emission peak (Figure 1). Following the approach of Bisschop et al.,[22] based on the occupation of the electron and hole levels, an amplitude can be assigned to the transition (i.e., completely empty levels yield an amplitude of +1, completely filled levels yield −1). Summing up all these Gaussians yields a nonlinear absorption spectrum that depends on the number of excitons in the system $\langle N \rangle$ (Figure S13, Supporting Information). We then derived the gain threshold spectrum by determining, for each wavelength, the number of excitons for which the spectra pass from absorption into gain. The results are shown in Figure 6e (sample B) and Figure 6f (sample A), respectively. Interestingly, line broadening leads to a further smoothening of the gain threshold spectra, here already observed at relatively lower temperature compared to the calculation using discrete energy levels. While

further work remains to be done to carefully disentangle both effects, we conclude that thermal occupation of holes should not be neglected when analyzing gain in colloidal nanocrystals, yet homo- and/or heterogeneous line broadening of the transitions can to a certain extent mask its effect.

3. Conclusions

In conclusion, combined experimental and computational work has revealed that the thermal occupation of excited hole states in CdSe/CdS giant-shell nanocrystals with a large core has a profound effect on both the excited-state bleach dynamics and the gain thresholds. The $k \cdot p$ calculations demonstrate that due to reduced quantum confinement in such CdSe/CdS nanocrystals, a large number of hole states is thermally accessible at room temperature, leading to long-lived bleach features in the transient absorption spectra. At the same time, the thermal occupation of these states, together with a sufficiently long band-edge gain lifetime approaching the nanosecond regime, yields a continuous, broadband gain spectrum up to 200 nm wide, spanning the entire spectral region between the CdSe and the CdS band edge. The gain threshold for the associated transitions, assigned again via $k \cdot p$ calculations, increases gradually with decreasing wavelength. This was confirmed by independently converting the gain lifetime into a gain threshold, assuming that the gain lifetime is limited by Auger recombination, and modeled by taking thermal occupancy of hole states into account in a state-filling model for the gain. Our results show that relaxing quantum confinement and therefore reducing the energetic spacing between the different hole states can lead to low-threshold broadband gain, and underline the role that temperature plays in such photophysics. The generality of the approach implies that it can be readily extended to future understanding of gain dynamics in similar colloidal nanocrystal systems, based for instance on III–V or perovskite semiconductors.

4. Experimental Section

Nanocrystal Synthesis: CdSe/CdS giant-shell nanocrystals were synthesized according to established procedures.[23] The characterization of the nanocrystals was reported by Di Stasio et al.[8]

Low-fluency transient absorption spectroscopy was conducted using samples in fused silica cuvettes, with solutions at a sufficiently low concentration to minimize variation in excitation density along the 1 mm optical path. The TA signal was collected in transmission geometry. An amplified Ti:sapphire laser (Quantronix Integra-C) generated 130 fs pulses centered at 800 nm, at a repetition rate of 1 kHz. A broadband UV–vis probe was generated by focusing the pulses into a thin CaF$_2$ plate, mounted on a moving stage to avoid laser-induced damage. For time delays up to 1 ns, the sample was excited with pump pulses centered at 400 nm, generated via second harmonic generation with pump-probe delay determined by a physical delay stage. For delays beyond 1 ns, pump pulses centered at 355 nm (700 ps FWHM) were obtained from the third harmonic of a Q-switched Nd:YVO$_4$ laser (Innolas Picolo) which was electronically triggered and synchronized to the Ti:sapphire laser via an electronic delay. After interaction with the sample, a homebuilt prism spectrometer dispersed the probe light onto a fast CCD array, enabling broadband shot-to-shot detection.

High-Fluency Transient Absorption Spectroscopy and Gain Measurements: Samples were photo-excited using 100 femtosecond pulses (1 kHz) at 400 and 530 nm, created from an 800 nm Ti:S laser (Spitfire Ace, Spectraphysics) through frequency mixing in a TOPAS optical parametric amplifier (Light Conversion). Broadband probe pulses were generated in a CaF2 (350–700 nm) using the 800 nm as seed. The probe was delayed using a delay stage with maximum delay of up to 3.3 ns (Newport TAS). Noise levels of 0.1 mOD (RMS) were obtained by averaging over 5000 shots per time delay. Using 2 mm path length cuvettes, the samples, diluted to an optical density of ≈0.2, were stirred during pump-probe measurements to avoid effects of photo-charging and sample degradation. No sample degradation was observed.

Quantification of Absorbed Photons Per Nanocrystal: The average number of absorbed photons (or photo-generated electron–hole pairs) at time zero, here labeled $\langle N \rangle$, generated by a pump pulse was calculated as $\langle N \rangle = J_{ph} \cdot \sigma_a$, with J_{ph} is the photon flux in photons cm^{-2} and σ_a is the absorption cross section of the nanocrystals. The beam size used for calculating J_{ph} is measured using a Thorlabs CCD Camera Beam profiler. The cross section is determined starting from the intrinsic absorption coefficient[29] as $\sigma_a = \mu_i \cdot V_{QD}$, with V_{QD} the average volume of a nanocrystal.

Gain Modeling and $k \cdot p$ Calculations: A full description of all calculations is given in the Supporting Information.

Supporting Information

Supporting Information is available from the Wiley Online Library or from the author.

Conflict of Interest

The authors declare no conflict of interest.

Data Availability Statement

The data that support the findings of this study are available from the corresponding author upon reasonable request.

[1] V. I. Klimov, A. A. Mikhailovsky, S. Xu, A. Malko, J. A. Hollingsworth, C. A. Leatherdale, H.-J. Eisler, M. G. Bawendi, *Science* **2000**, *290*, 314.

**ADVANCED
SCIENCE NEWS**

www.advancedsciencenews.com

**ADVANCED
OPTICAL
MATERIALS**

www.advopticalmat.de

[2] V. I. Klimov, A. A. Mikhailovsky, D. W. McBranch, C. A. Leatherdale, M. G. Bawendi, *Science* **2000**, *287*, 1011.

[3] Y.-S. Park, J. Lim, N. S. Makarov, V. I. Klimov, *Nano Lett.* **2017**, *17*, 5607.

[4] M. M. Adachi, F. Fan, D. P. Sellan, S. Hoogland, O. Voznyy, A. J. Houtepen, K. D. Parrish, P. Kanjanaboos, J. A. Malen, E. H. Sargent, *Nat. Commun.* **2015**, *6*, 8694.

[5] F. Fan, O. Voznyy, R. P. Sabatini, K. T. Bicanic, M. M. Adachi, J. R. McBride, K. R. Reid, Y.-S. Park, X. Li, A. Jain, R. Quintero-Bermudez, M. Saravanapavanantham, M. Liu, M. Korkusinski, P. Hawrylak, V. I. Klimov, S. J. Rosenthal, S. Hoogland, E. H. Sargent, *Nature* **2017**, *544*, 75.

[6] O. V. Kozlov, Y.-S. Park, J. Roh, I. Fedin, T. Nakotte, V. I. Klimov, *Science* **2019**, *365*, 672.

[7] J. J. Geuchies, B. Brynjarsson, G. Grimaldi, S. Gudjonsdottir, W. van der Stam, W. H. Evers, A. J. Houtepen, *ACS Nano* **2021**, *15*, 377.

[8] F. D. Stasio, A. Polovitsyn, I. Angeloni, I. Moreels, R. Krahne, *ACS Photonics* **2016**, *3*, 2083.

[9] M. Nasilowski, P. Spinicelli, G. Patriarche, B. Dubertret, *Nano Lett.* **2015**, *15*, 3953.

[10] F. Garcia-Santamaria, Y. Chen, J. Vela, R. D. Schaller, J. A. Hollingsworth, V. I. Klimov, *Nano Lett.* **2009**, *9*, 3482.

[11] V. Pinchetti, F. Meinardi, A. Camellini, G. Sirigu, S. Christodoulou, W. K. Bae, F. De Donato, L. Manna, M. Zavelani-Rossi, I. Moreels, V. I. Klimov, S. Brovelli, *ACS Nano* **2016**, *10*, 6877.

[12] K. E. Shulenberger, S. C. Coppieters 't Wallant, M. D. Klein, A. R. McIsaac, T. Goldzak, D. B. Berkinsky, H. Utzat, U. Barotov, T. Van Voorhis, M. G. Bawendi, *Nano Lett.* **2021**, *21*, 7457.

[13] P. Kambhampati, *J. Phys. Chem. C* **2011**, *115*, 22089.

[14] C. Melnychuk, P. Guyot-Sionnest, *Chem. Rev.* **2021**, *121*, 2325.

[15] R. Koole, G. Allan, C. Delerue, A. Meijerink, D. Vanmaekelbergh, A. J. Houtepen, *Small* **2008**, *4*, 127.

[16] M. G. Lupo, F. Della Sala, L. Carbone, M. Zavelani-Rossi, A. Fiore, L. Luìˆer, D. Polli, R. Cingolani, L. Manna, G. Lanzani, *Nano Lett.* **2008**, *8*, 4582.

[17] A. W. Achtstein, A. V. Prudnikau, M. V. Ermolenko, L. I. Gurinovich, S. V. Gaponenko, U. Woggon, A. V. Baranov, M. Y.u. Leonov, I. D. Rukhlenko, A. V. Fedorov, M. V. Artemyev, *ACS Nano* **2014**, *8*, 7678.

[18] S. L. Chuang, C. S. Chang, *Phys. Rev. B* **1996**, *54*, 2491.

[19] J. Planelles, F. Rajadell, J. I. Climente, *J. Phys. Chem. C* **2010**, *114*, 8337.

[20] C. Segarra, J. I. Climente, A. Polovitsyn, F. Rajadell, I. Moreels, J. Planelles, *J. Phys. Chem. Lett.* **2016**, *7*, 2182.

[21] G. Grimaldi, J. J. Geuchies, W. van der Stam, I. du Fossé, B. Brynjarsson, N. Kirkwood, S. Kinge, L. D. A. Siebbeles, A. J. Houtepen, *Nano Lett.* **2019**, *19*, 3002.

[22] S. Bisschop, P. Geiregat, T. Aubert, Z. Hens, *ACS Nano* **2018**, *12*, 9011.

[23] S. Christodoulou, G. Vaccaro, V. Pinchetti, F. D. Donato, J. Q. Grim, A. Casu, A. Genovese, G. Vicidomini, A. Diaspro, S. Brovelli, L. Manna, *J. Mater. Chem. C* **2014**, *2*, 3439.

[24] W. K. Bae, L. A. Padilha, Y.-S. Park, H. McDaniel, I. Robel, J. M. Pietryga, V. I. Klimov, *ACS Nano* **2013**, *7*, 3411.

[25] I. Robel, R. Gresback, U. Kortshagen, R. D. Schaller, V. I. Klimov, *Phys. Rev. Lett.* **2009**, *102*, 177404.

[26] J. I. Climente, J. L. Movilla, J. Planelles, *J. Appl. Phys.* **2012**, *111*, 043509.

[27] J. P. Philbin, E. Rabani, *Nano Lett.* **2018**, *18*, 7889.

[28] J. P. Philbin, E. Rabani, *J. Phys. Chem. Lett.* **2020**, *11*, 5132.

[29] I. Angeloni, W. Raja, R. Brescia, A. Polovitsyn, F. De Donato, M. Canepa, G. Bertoni, R. Proietti Zaccaria, I. Moreels, *ACS Photonics* **2016**, *3*, 58.